LANGMUIR

pubs.acs.org/Langmuir Article

Spontaneous Deposition of Single Platinum Atoms on Anatase TiO_2 for Photocatalytic H_2 Evolution

Published as part of Langmuir virtual special issue "2023 Pioneers in Applied and Fundamental Interfacial Chemistry: Janet A. W. Elliott".

Kenza Toukabri,[#] Sina Hejazi,[#] Majid Shahsanaei, Sadegh Pour-Ali, Ali Kosari, Benjamin Butz, Manuela Sonja Killian,* and Shiva Mohajernia*

Cite This: *Langmuir* 2024, 40, 4661−4668 Read Online

ACCESS | Metrics & More | Article Recommendations

ABSTRACT: Single-atom (SA) decoration has emerged as a frontier in catalysis due to its unique characteristics. Recently, decorated Pt single atoms on titania have shown promise in photocatalytic hydrogen evolution. In this work, we demonstrate that Pt SAs can spontaneously deposit on the surface, driven by electrostatic forces; the key is to determine the golden pH and surface potential. We conducted a comprehensive investigation into the influence of the pH of the deposition precursor on the spontaneous adsorption of Pt SAs onto TiO_2 nanosheets (TiNSs). We introduced a straightforward pH-dependent and charge-dependent strategy for the solid electrostatic anchoring of Pt SAs on TiO_2. Furthermore, we established that the level of Pt loading can be controlled by adjusting the precursor pH. X-ray photoelectron spectroscopy (XPS) and high-angle annular dark-field imaging scanning transmission electron microscopy (HAADF-STEM) were used to evaluate the Pt SA-decorated samples. Photocatalytic hydrogen production activity was assessed under ultraviolet (UV) (365 nm) irradiation. Notably, we found that at a pH of 8, slightly below the measured point of zero charge (PZC), a unique mixture of Pt clusters and single atoms was deposited on the surface of TiNSs. This unique composition significantly improved hydrogen production, resulting in ∼3.7 mL of hydrogen generated after 8 h of UV exposure by only 10 mg of the Pt-decorated TiNS (with Pt loadings of 0.12 at. %), which is ∼300 times higher than the undecorated TiNS.

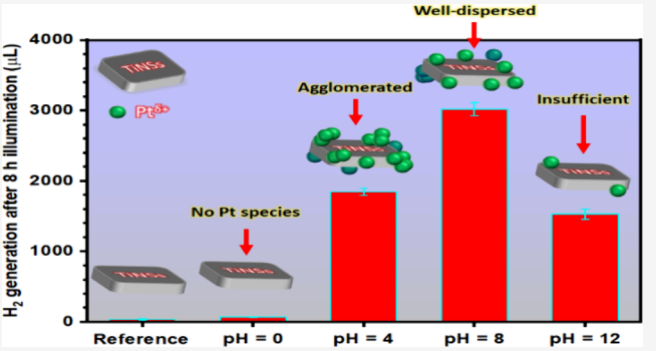

INTRODUCTION

Single-atom catalysts (SACs) have recently gained prominence as a frontier in catalysis due to their unique advantages, including exceptional activity and selectivity.[1−4] SACs bridge the gap between heterogeneous and homogeneous catalysis, harnessing the atom efficiency of metals to enhance the utilization of noble metals. They exhibit low coordination environments stemming from unsaturated bonding, facilitating efficient charge transfer. Additionally, SACs manifest distinct highest occupied molecular orbitals−lowest unoccupied molecular orbital (HOMO−LUMO) gaps due to quantum size effects, providing exceptional catalytic properties.[4−9]

Metal oxides, including TiO_2, are among the most suitable photocatalysts and are ideal supports for SACs. Their properties encompass acidity, either Lewis or Bronsted types, and basicity, influencing the nature of anchored metal groups.[10,11] Anchoring SACs on metal oxide supports necessitates robust bonding interactions, such as covalent metal−support interaction (CMSI) and electronic metal−support interaction (EMSI).[12] Researchers have harnessed CMSI to stabilize Au_1 SACs on FeO_x support through covalent Au_1−FeO_x interactions.[13] Similarly, CMSI effects have been observed by dispersing Pt clusters on a CeO_2 support, resulting in electronic interactions between Pt clusters and CeO_2.[14,15] The surface chemistry of metal oxides, specifically the presence of hydroxyl groups or oxygen ions at the surface, allows for potential stabilization of SACs through M−O(OH) interactions.[12] Moreover, metal oxide supports exhibit diverse defect types, including oxygen vacancies (V_O) and metal vacancies (V_M), deliberately introduced as favorable anchoring

Received: October 31, 2023
Revised: January 24, 2024
Accepted: January 29, 2024
Published: February 20, 2024

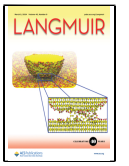

https://doi.org/10.1021/acs.langmuir.3c03316
Langmuir 2024, 40, 4661−4668

sites for SACs, as well as surface morphology defects like kinks, steps, and terraces, which may trap SACs.[9,16]

To achieve stable, high-loading, and well-dispersed SACs on support materials, a profound understanding of SACs' adsorption behavior on the support surface is crucial. Surface polarization of oxides in relation to pH and electrostatic attraction-mediated adsorption of counterions are crucial factors governing SAC deposition. Therefore, monitoring the point of zero charge (PZC) of the oxide, the pH of the aqueous solution, and the metallic complex's nature is pivotal for successful SAC deposition. Amphoteric metal oxides in solution tend to polarize and acquire electrical charges contingent upon the pH of the solution.[17,18] According to the electroneutrality principle, counterions closely associate with metal oxide particles in a thin, diffuse layer, as per Gouy's theory. In acidic solutions, metal oxides are positively charged and surrounded by compensating anions, while in basic solutions, negatively charged metal oxides are encircled by compensating cations. At the PZC or the isoelectric point (IEP), the surface displays a neutral charge. The PZC of a metal oxide may vary upon the exact production method. Surface charges critically influence the adsorption of metal ions or complexes due to the Coulombic nature of the adsorption process. Depending on the solution's pH, various species may form on the surface, including monolayers of H^+, neutral water molecules adsorbing on metal sites (H_2O_M), hydroxylated metal sites (OH_M^-), and free surface oxygen atoms.[19−21]

TiO_2, specifically in its anatase polymorph, has been extensively chosen as the preferred support for SACs. This selection is attributed to TiO_2's distinctive photocatalytic properties, which include cost-effectiveness, abundance, well-suited band positions for water splitting, resistance to photocorrosion, and high chemical stability.[22−24] It is widely acknowledged that defects on the support surface play an indisputable role in trapping single-atoms (SAs) and have consistently been identified as the preferred sites for SAs adsorption. A fundamental aspect of controlling SAs decoration hinges on comprehending the spontaneous adsorption of SAs on the support material's surface, a parameter intricately linked with the material's PZC.[25,26] Despite the studies exploring defect-engineered surfaces, the potential for spontaneous self-adsorption of Pt SAs on anatase surfaces has remained largely unaddressed in the literature. In the present study, we performed a systematic investigation of the pH-dependent adsorption of Pt SAs on anatase TiO_2 nanosheets (TiNSs) as the support material. While the decoration of titania with noble metal SAs has recently become a frontier in photocatalysis research, the influence of the PZC on the adsorption of SAs and clusters, which represents a pivotal aspect of SAs adsorption studies, has been overlooked.

EXPERIMENTAL METHOD

Synthesis of Anatase TiO_2 Nanosheets (TiNSs). Anatase TiNSs were synthesized using a hydrothermal method as previously reported.[27] The reagents, tetrabutyl titanate ($Ti(OBu)_4$) and concentrated hydrofluoric acid (HF, 48%) from Sigma−Aldrich Merck, were used as received without further purification. To prepare the TiNSs, 10 mL of $Ti(OBu)_4$ was added dropwise to 1.2 mL of HF in a 250 mL Teflon liner while stirring at room temperature. After 40 min of agitation, the Teflon liner was sealed in an autoclave and placed in an oven preheated to 200 °C. Following 24 h of hydrothermal reaction, the autoclave was allowed to cool in the oven. The resulting precipitates were collected by centrifugation (Heraeus SEPATECH), washed repeatedly with distilled water and ethanol, and dried overnight at 75 °C.

Pt Decoration Process. Chemical bath deposition method was used to decorate Pt on TiO_2−NSs. The starting solution (mother solution) was a 2.4 mM solution of H_2PtCl_6 that was prepared using dihydrogen hexachloroplatinate(IV) hydrate $H_2PtCl_6{\cdot}xH_2O$ (99.9%; Sigma−Aldrich). The mother solution was diluted 10 times (in a 100 mL container) to obtain a 240 μM H_2PtCl_6 solution. This was done to ensure a more precise measurement of the weight value of H_2PtCl_6 powder. To ensure the solution was completely homogeneous, it was prepared by dilution and made completely uniform. To achieve the desired pH level separately prepared diluted sulfuric acid or KOH solutions were added dropwise to each solution. The final volume of each solution was adjusted to 200 mL. Therefore, all solutions had a final concentration of 120 μM H_2PtCl_6. Next, 50 mg of nanosheets were added to each container and sonicated for 2 min, then stirred on a magnetic stirrer for 1 h. The resulting powder was then transferred to a 200 cm^3 centrifuge tube and centrifuged at 4000 rpm. The separated solution was removed, and 200 cm^3 of water was added to the centrifuge tube. This process of centrifugation and water washing was repeated three times. The powder was then taken out of the centrifuge tube and transferred to a paper filter. After washing the powder with 50 cm^3 of water, it was transferred to an oven at 40 °C and left overnight to remove any residual water. To establish a correlation between the Pt decoration and PZC of TiNSs, zeta potential was determined using a zetasizer across the pH range of 0 to 12.

Characterization of Nondecorated and Pt-Decorated TiNSs. The synthesized TiNSs were characterized using high-resolution transmission electron microscopy (HRTEM) (FEI Talos F200X). Samples of Pt-decorated TiNSs were investigated using high-angle annular dark-field scanning transmission electron microscopy (HAADF-STEM) and HRTEM with a Thermofisher Spectra Ultra TEM (TEAM 1) operating at 300 kV. The chemical state and loading of the Pt SAs were characterized using X-ray photoelectron spectroscopy (XPS) with a Surface Science Instrument (SSX-100 S-probe), employing K_α radiation at 200 W. High-resolution XPS spectra were recorded with a 0.2 eV energy resolution and a spot size of 300 μm^2, with peak positions calibrated to the C 1s peak at 284.8 eV.

Measurement of Hydrogen Production Rate. The hydrogen production rate was measured using a gas chromatograph (SRI, Model 8610C, TCD-detector) with a quartz photoreactor. Initially, 10 mg of TiNSs powder or Pt-decorated TiNSs were stirred in a 20 mL solution of distilled water and methanol (1:1) for 15 min under nitrogen gas purging to remove oxygen, then carefully sealed. The mixture inside the photoreactor was sonicated for 15 min for more homogeneous dispersion. Stirring was maintained during light irradiation to prevent potential precipitation. A 365-nm LED light source (680 mW cm^{-2}, SPCM-0800, DUSA) was used for 24 h of illumination.

Electrochemical Impedance Spectroscopy (EIS) Measurements. Based on a study by Obradović et al., stable electrodes from pristine and Pt-loaded TiNSs were prepared to conduct the EIS measurements.[28] In this procedure, 10 mg of the corresponding TiNSs were first added to 4 mL of double-distilled water and the suspension was sonicated for 45 min at room temperature. Subsequently, 200 μL of Nafion perfluorinated resin were added to the suspension and the mixture was agitated for 45 min. Finally, 240 μL of the suspension were spread over the surface of a glassy carbon disk and the disk was oven-dried at 60 °C for 60 min. The EIS measurements were performed using a PalmSens4 potentiostat with a conventional three-electrode cell: the glassy carbon disc coated with the catalytic layer as the working electrode, a platinum plate as the counter electrode, and Ag/AgCl as the reference electrode. The data were recorded within the frequency range of 10 kHz to 10 mHz by applying a sinusoidal perturbing signal of 5 mV around the open circuit potential. The measurements were carried out in 0.5 M H_2SO_4 solution at 26 ± 1 °C. The data reproducibility of each test was checked by triplicate repetition.

https://doi.org/10.1021/acs.langmuir.3c03316
Langmuir 2024, 40, 4661−4668

RESULTS AND DISCUSSION

The morphology of the TiNSs synthesized in their pristine state is shown in Figures 1a–c. A substantial portion of these

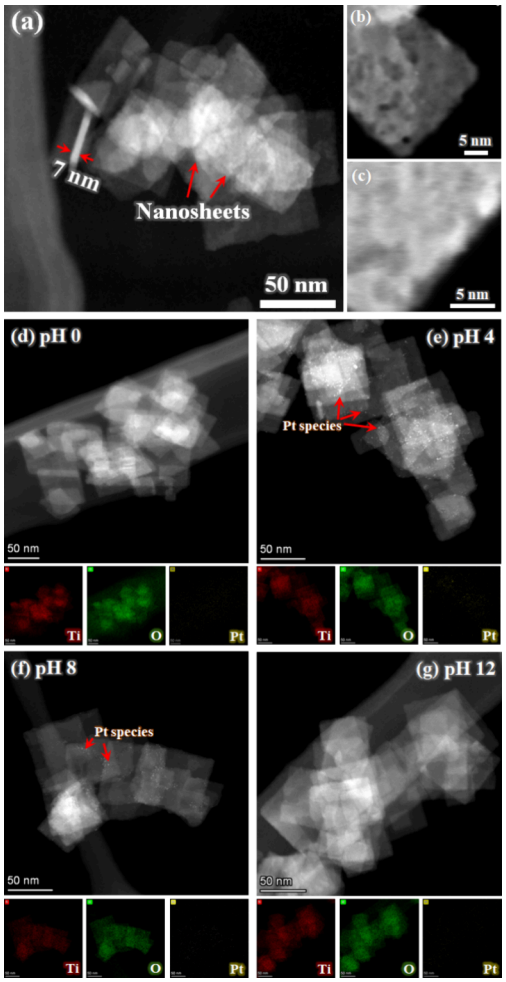

Figure 1. (a–c) HRTEM image of pristine TiNSs with various magnifications; HAADF-TEM images of TiNSs subjected to various pH conditions ((d) 0, (e) 4, (f) 8, and (g) 12).

nanosheets exhibits a clearly defined sheetlike structure characterized by a rectangular shape, with side dimensions ranging from ∼30 nm to 60 nm and an average thickness of ∼7 nm. Figures 1d–g illustrate the HAADF-TEM images of TiNSs subjected to pH conditions of 0, 4, 8, and 12. When compared to the pristine TiNSs, the presence of Pt SAs and Pt atom assemblies is discernible exclusively on the surfaces of TiNSs treated at pH levels of 4 and 8. It is noteworthy that, following treatment at varying pH values, there is no observable alteration in the dimensions of the TiNSs (Figure 1g), underscoring the preservation of the nanosheets structure.

To analyze the chemical state of Pt atoms on TiNSs, XPS examination was conducted. Figure 2a displays the XPS survey spectra of TiNSs subjected to varying pH conditions. The XPS survey results reveal the predominant presence of elements such as Ti, F, O, and carbon contaminants. The absence of Cl 2p peaks in the samples suggests that the Pt signals originate from Pt atoms rather than remnants of the precursor material. The XPS data within the binding energy range of 80–68 eV support the findings from HAADF-TEM analysis (Figure 2b). Specifically, the XPS intensities of Pt 4f in samples treated at pH levels of 4 and 8 are notably several times greater than those in samples subjected to pH conditions of 0 and 12. The assessment and comparison of Pt loading on the TiNS surface, as influenced by different pH levels, were carried out using quantitative XPS, as depicted in Figure 2c. The XPS outcomes reveal that, under highly acidic conditions (pH 0), no detectable Pt deposition occurs. However, as the pH is increased, Pt species deposition occurs. Comparing the measured samples, the highest observed level of Pt deposition on the TiNS surface is recorded at pH 4, reaching ∼0.24 at. %. With an increase in pH to 8, there is a slight reduction in Pt loading (∼0.15 at. %). Notably, under highly alkaline conditions, such as pH 12, a significant decrease in Pt loading is observed (∼0.02 at. %).

Reflectance spectroscopy (DRS) is uttilized to examine how the light absorption properties of TiO_2–NSs are affected by Pt decoration. The results for both the reference TiO_2-NSs and the sample treated at pH 8 are shown in Figures 2d and 2e. Our analysis revealed that the bandgap values for these samples are 3.28 and 3.23 eV, respectively. It is important to note that there is very little difference in the bandgap and whole absorption spectrum between these two samples. In other words, any potential difference in photocatalytic activity between pt decorated and pristine samples cannot be attributed to differences in light absorption.

As a result of the substantial quantities of Pt decoration observed on TiNSs prepared at pH 4 and pH 8, further investigations were carried out via HRTEM and high-resolution XPS on these samples. Figures 3a and 3b present a comparative HRTEM analysis of the Pt species' size and their spatial distribution on the surface of TiNSs subjected to treatments at pH 4 and pH 8. The results reveal slightly larger Pt particles at pH 4, compared to those at pH 8, suggesting a preferential formation of Pt nanoparticles at pH 4 and formation of a combination of Pt SAs and Pt clusters at pH 8. Additionally, as shown in Figures 3c and 3d, our statistical analysis based on HAADF-STEM images further supports these findings. Figure 3c illustrates the quantification of single atom counts per 100 nm^2 across different pH values, highlighting higher single atom density at pH 8. Meanwhile, Figure 3d showcases the percentage of area occupied by clusters/agglomerates relative to the total area, elucidating higher Pt agglomeration at pH 4. Thus, pH proves to be an important factor for Pt SAs decoration and distribution on support materials. In addition, as shown in Figures 3c and 3d, the deconvolution of high-resolution XPS spectra reveals that the binding energies of the Pt 4f signal correspond to oxidized Pt.[29] The pH 4 sample exhibits an additional shoulder that is indicative of metallic Pt. For the pH 8 sample, the Pt 4f peak can be deconvoluted into four distinct peaks. The signals at 72.44 and 75.88 eV correspond to Pt^{2+} $4f_{7/2}$ and Pt^{2+} $4f_{5/2}$, respectively, while the doublet at 74.4 and 77.39 eV can be attributed to Pt^{4+} $4f_{7/2}$ and Pt^{4+} $4f_{5/2}$. In contrast, for the pH 4 sample, the deconvolution requires inclusion of the metallic state, featuring signals at 71.68 and 75.27 eV corresponding to Pt^0 $4f_{7/2}$ and Pt^0 $4f_{5/2}$, respectively. Furthermore, two doublets for Pt oxide are observed in this sample, with peaks at 72.51 and 75.90 eV attributed to Pt^{2+} $4f_{7/2}$ and Pt^{2+} $4f_{5/2}$. Therefore, the XPS results provide further evidence for the atomic-scale deposition of Pt on the pH 8-treated TiNS, while for the pH 4-treated TiNS, a combination of metallic bonds originating from Pt nanoparticle formation and atomic-scale deposition of Pt is evident. Consistent with existing literature, the deposition

https://doi.org/10.1021/acs.langmuir.3c03316
Langmuir 2024, 40, 4661–4668

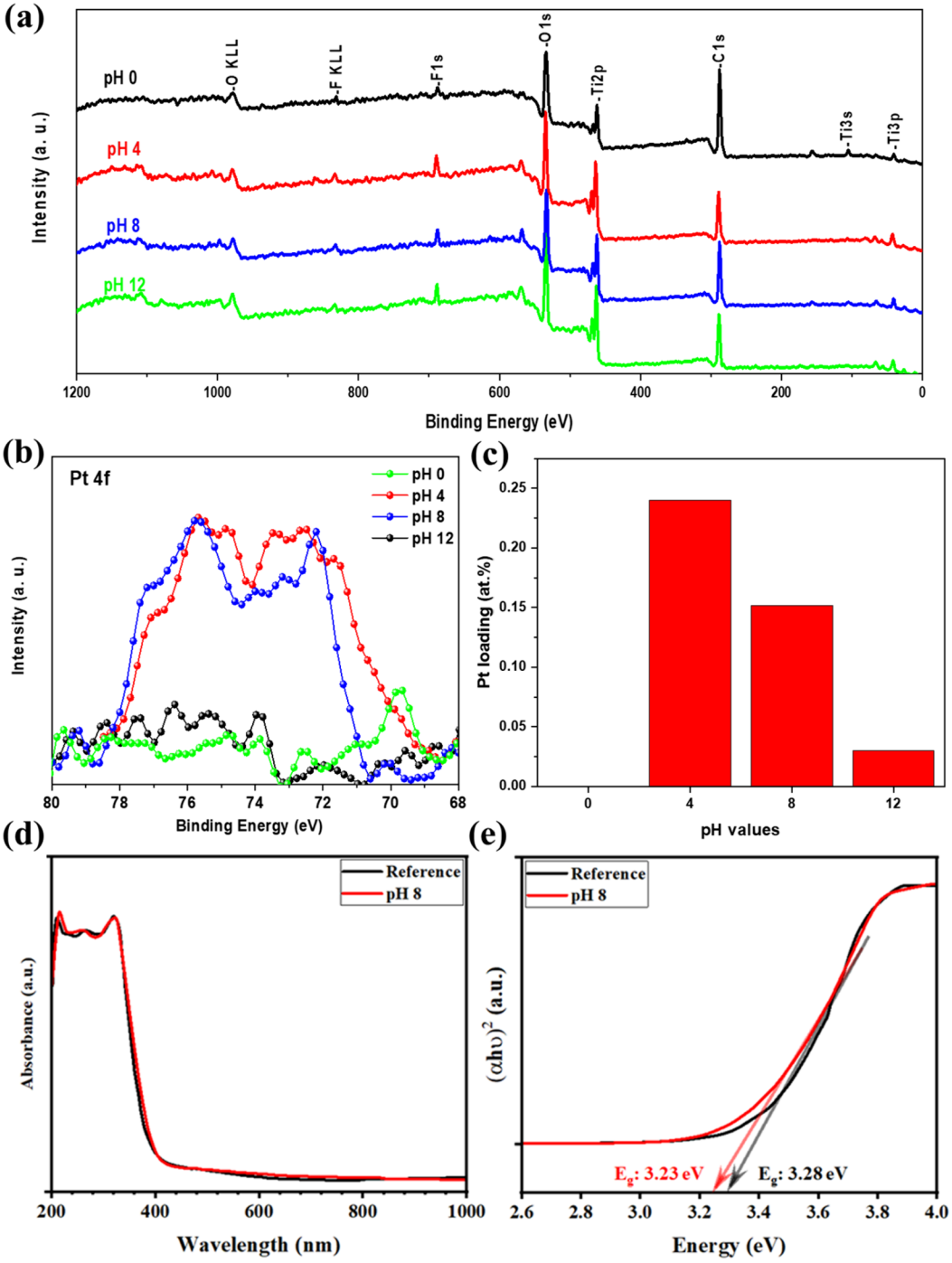

Figure 2. (a) Overall XPS survey spectra of the prepared TiNS in various pH; (b) Pt 4f XPS spectra for different TiNSs samples; (c) Pt loading on the surface of anatase TiNSs prepared at different pH values, as determined by XPS; (d) absorbance spectra and (e) Tauc plots of the reference TiO_2−NSs and the samples treated at pH 8.

of SAs results in species coordination to their surrounding environment, primarily involving oxygen atoms in the case of oxide supports.[30−33] Consequently, a shift toward higher binding energies is observed. Moreover, the presence of high-valent Pt^{4+} combined with the absence of Cl^- suggests a strong covalent interaction between Pt and the TiO_2 support, predominantly observed in the pH 8-treated TiNS.

The photocatalytic performance of the samples treated in Pt-containing solutions with varying pH levels was evaluated for hydrogen (H_2) evolution under UV light irradiation. The results, presented in Figure 4a, reveal that the sample treated at pH 8 demonstrates the highest photocatalytic H_2 generation activity, achieving a rate of ∼3.75 mL h^{-1} g^{-1}. To assess the reusability of this sample, successive photocatalytic H_2 generation experiments were conducted under identical conditions. Figure 4b illustrates that the activity of this sample remains consistent, showing no significant decrease even after four consecutive 8-h cycles. This observation indicates an ∼83% retention in the stability of H_2 evolution, highlighting the remarkable stability of Pt sites on the TiO_2−NSs. Combining the HAADF-TEM and XPS findings, we propose that the presence of a combination of Pt SAs and Pt SA

https://doi.org/10.1021/acs.langmuir.3c03316
Langmuir 2024, 40, 4661−4668

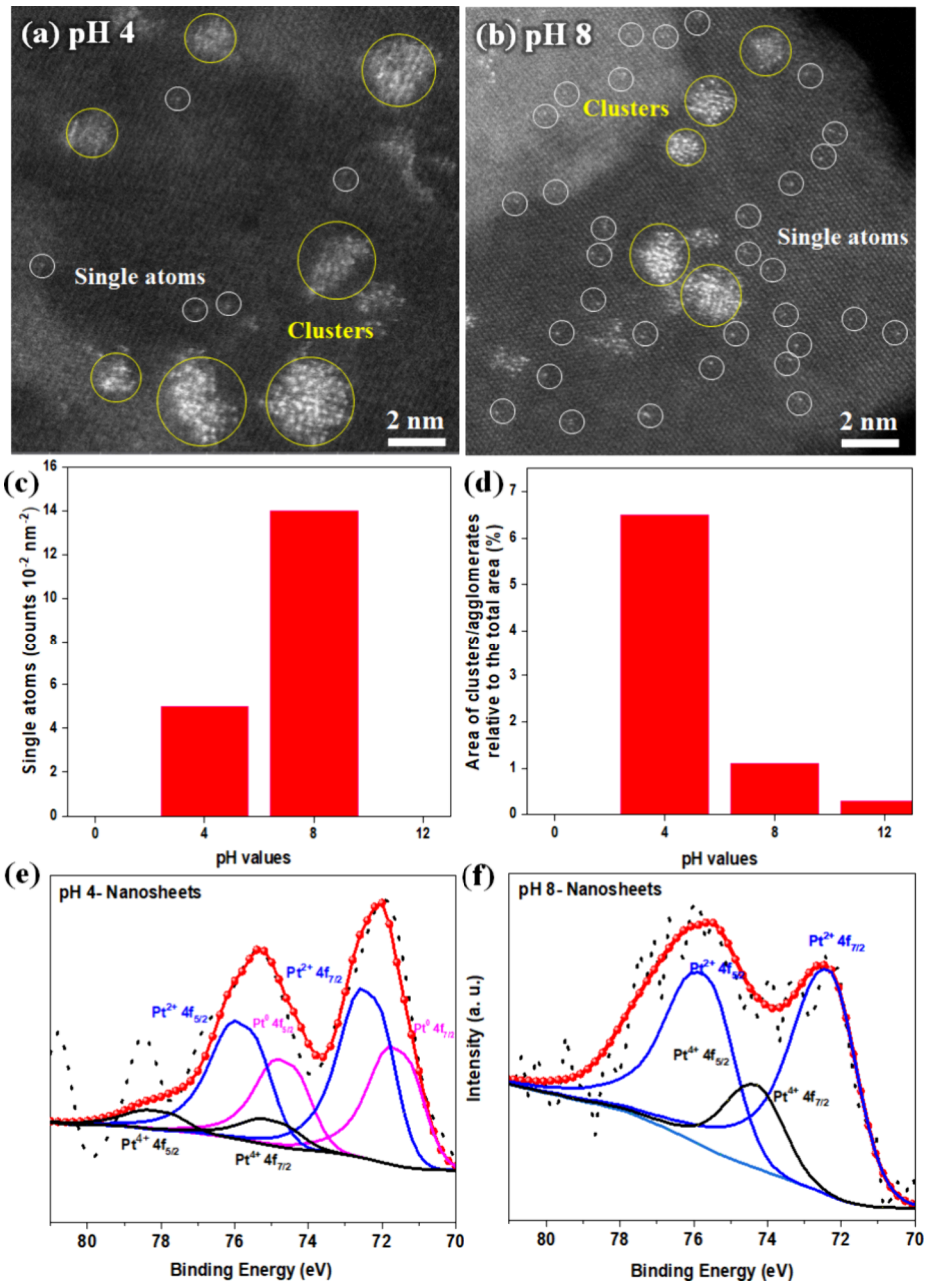

Figure 3. HAADF-STEM images of Pt-decorated anatase TiNSs prepared at (a) pH 4 and (b) pH 8. Surface density of (c) Pt single atoms and (d) Pt clusters/agglomerates for different samples. High-resolution XPS spectra of Pt 4f of anatase TiNSs at (e) pH 4 and (f) pH 8.

assemblies, exhibiting greater uniformity across the TiNSs surface, is pivotal for achieving highly efficient and stable SA catalysts. Our results align with recent reports highlighting the enhanced heterogeneous catalytic efficiency achieved by the simultaneous presence of SAs and SA assemblies (clusters) on a support material, compared to the presence of individual components.[30]

EIS can also provide insights into the charge transfer kinetics of TiO_2-based samples.[34,35] Figure 4c–e shows the EIS results for the pristine and Pt-decorated TiNSs prepared at different pH, which was measured at open circuit potential. While the impedance values may vary across the different samples, they are consistently identified by a semicircle at higher to midrange frequencies, and an arc-shaped pattern at lower frequency ranges (Figure 4c). The semicircle is related to the electrical double layer at the TiO_2/solution interface and the arc can be explained by the formation of a space charge layer, which indicates the accumulation of charge carriers within the TiO_2 material. Nyquist plots reveal that the Pt-decorated TiNS prepared at pH 8 possess the smallest diameter, indicating the lowest polarization resistance among all samples. Furthermore, this sample exhibits lower impedance at a frequency of 0.01 Hz in the Bode modulus, and lower phase angles in the Bode phase plot, which are indicative of its superior electron transfer properties at the interface between TiO_2 and the solution. To conduct a quantitative analysis of the EIS results, the experimental data were fitted to an equivalent circuit, which is depicted in Figure 4c (inset). In this circuit, R_s, R_p, and CPE_{dl} are the solution resistance, polarization resistance, and constant phase element regarding the electrical double layer, respectively. Moreover, R_{SC} and CPE_{SC} are the space charge resistance and the constant phase element regarding the space

https://doi.org/10.1021/acs.langmuir.3c03316
Langmuir 2024, 40, 4661−4668

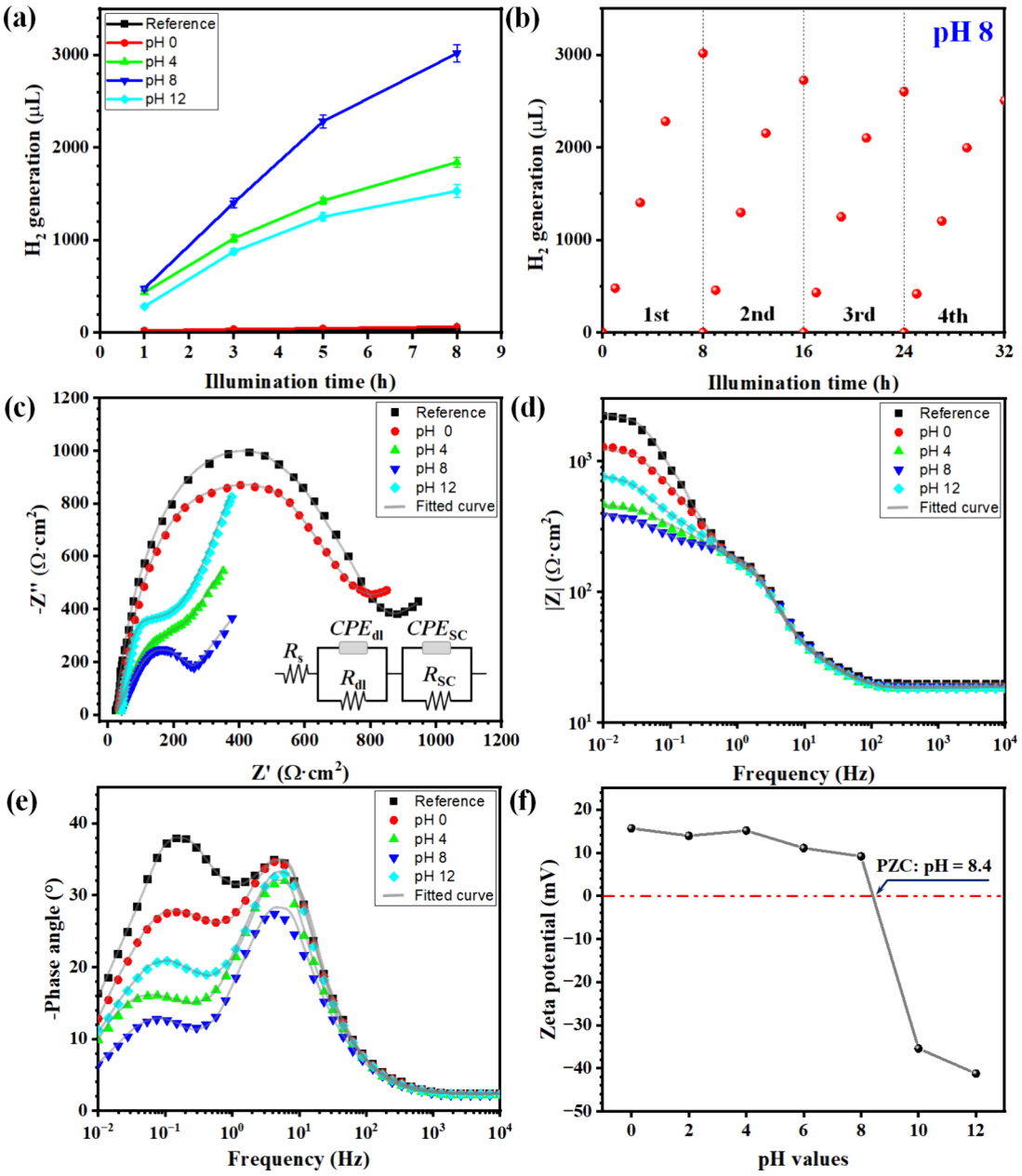

Figure 4. (a) H_2 evolution of 10 mg Pt decorated anatase TiNSs at different pH values; (b) reusability experiment for photocatalytic H_2 generation of the sample treated at pH = 8; (c) Nyquist plot with equivalent circuit used for the fitting of EIS data (inset); (d) Bode-modulus, and (e) Bode-phase plots of various samples; (f) zeta potentials of the TiNSs at different pHs. pH_{PZC} (point zero of charge) of TiNSs is ∼8.4.

Table 1. Equivalent Circuit Parameters for the EIS Data of Different Samples

			CPE_{dl}			CPE_{SC}		
sample	R_s (Ω cm^2)	R_p (Ω cm^2)	n_{dl}	$Y_{0,dl}$ (× 10^{-6} S s^n cm^{-2})	R_{SC} (Ω cm^2)	n_{SC}	$Y_{0,SC}$ (× 10^{-6} S s^n cm^{-2})	χ^2
reference	16.2	475	0.92	11	1675	0.90	24	0.0005
pH 0	14.5	422	0.90	13	1036	0.89	27	0.0004
pH 4	15.4	237	0.88	22	191	0.93	35	0.0007
pH 8	16.5	203	0.90	30	138	0.92	41	0.0009
pH 12	16.1	313	0.91	18	409	0.90	30	0.0001

charge layer. It is noteworthy that the *CPE* represents a nonideal capacitance, which is characterized by the parameters Y_0 and n, signifying the magnitude and deviation of the CPE, respectively. The results of the data fitting process are presented in Table 1. As the n values for all samples fall between 0.5 and 1.0, it can be inferred that the CPEs exhibit capacitive behavior. In comparison to the other samples, the Pt-decorated TiNS prepared at pH 8 show the lowest R_p and R_{SC} values, indicating superior electron transfer and reduced electron accumulation.

To establish a correlation between Pt decoration and the surface charge of TiNSs in various solutions, we recorded and

https://doi.org/10.1021/acs.langmuir.3c03316
Langmuir 2024, 40, 4661−4668

plotted the zeta potentials of TiNSs at different pH levels, as illustrated in Figure 4f. As the pH surpasses the PZC (pH_{PZC} ~8.4), the TiNSs surface becomes negatively charged. Consequently, adsorption of anionic complexes, stable during the hydrolysis of $[PtCl_6]^{2-}$, becomes unfeasible. However, under highly acidic conditions, despite the positively charged TiNSs surface, strong adsorption of chloroaqua complexes (such as $[PtCl_5(H_2O)]^-$) onto TiNSs is anticipated. Yet, the high stability of these complexes at pH such as 0 impedes their deposition. Under these acidic conditions, these complexes mainly exhibit negative solvation-free energy, enhancing their tendency to remain in solution rather than adhere to the metal oxide surface. This affinity diminishes as pH surpasses 4. Moreover, at pH >7, increased hydroxide ions lead to water molecule deprotonation, fostering the formation and subsequent adsorption of hydroxo complexes (such as $[PtCl_5(OH)]^{2-}$, $[PtCl_4(OH)(H_2O)]^-$, and $[PtCl_4(OH)_2]^{2-}$).[20,36−38] Consequently, the presence of Pt SAs and Pt SA assemblies becomes more pronounced at pH 8, which is in close proximity to the measured PZC of the TiNSs. This observation along with the HAADF-TEM and XPS results collectively highlight the significance of the pH-dependent Pt decoration process on TiNSs, elucidating the complex interaction between surface charge, Pt adsorption, and the formation of Pt SAs and Pt SA assemblies on the surface.

CONCLUSIONS

We systematically investigated the critical influence of pH on the atomic-scale deposition of Pt onto TiNSs. Our findings illuminate the significantly overlooked yet paramount role of the deposition solution's pH in the decoration process of Pt SAs and Pt SA assemblies. We have demonstrated a strong pH dependence in the Pt decoration process, with the most promising results observed at a specific pH of 8. It is noteworthy that extreme pH conditions, both highly acidic and highly basic, present significant challenges to the Pt decoration process. The stability of the $[PtCl_6]^{2-}$ complex under very acidic conditions and the repulsion between the complex and the TiNSs surface under highly basic conditions hindered the efficient Pt decoration process. At a pH of 8, we achieved a highly active combination of Pt SAs and Pt clusters. We showed that the mixture of Pt species, including Pt SAs and Pt clusters with higher oxidized forms (Pt^{2+} and Pt^{4+}), emerged as the key contributor to the exceptional photocatalytic efficiency. Notably, we achieved a remarkable H_2 generation rate of 3.75 mL h^{-1} g^{-1}.

AUTHOR INFORMATION

Corresponding Authors

Manuela Sonja Killian − *Chemistry and Structure of Novel Materials, Department of Chemistry and Biology, University of Siegen, 57076 Siegen, Germany;* orcid.org/0000-0003-0892-4614; Email: manuela.killian@uni-siegen.de

Shiva Mohajernia − *Chemistry and Structure of Novel Materials, Department of Chemistry and Biology, University of Siegen, 57076 Siegen, Germany; Department of Chemical and Materials Engineering, Faculty of Engineering, University of Alberta, Edmonton T6G 1H9 Alberta, Canada;* orcid.org/0000-0002-0194-0286; Email: mohajernia@ualberta.ca

Authors

Kenza Toukabri − *Chemistry and Structure of Novel Materials, Department of Chemistry and Biology, University of Siegen, 57076 Siegen, Germany*

Sina Hejazi − *Chemistry and Structure of Novel Materials, Department of Chemistry and Biology, University of Siegen, 57076 Siegen, Germany;* orcid.org/0000-0003-1526-5629

Majid Shahsanaei − *Chemistry and Structure of Novel Materials, Department of Chemistry and Biology, University of Siegen, 57076 Siegen, Germany*

Sadegh Pour-Ali − *Faculty of Materials Engineering, Sahand University of Technology, 51335-1996 Tabriz, Iran;* orcid.org/0000-0002-3748-5764

Ali Kosari − *Debye Institute for Nanomaterials Science, Universiteit Utrecht, NL 3548CC Utrecht, The Netherlands*

Benjamin Butz − *Mechanical Engineering, University of Siegen, 57076 Siegen, Germany;* orcid.org/0000-0002-9744-3419

Complete contact information is available at: https://pubs.acs.org/10.1021/acs.langmuir.3c03316

Author Contributions

#K.T. and S.H. contributed equally to this work.

Notes

The authors declare no competing financial interest.

ACKNOWLEDGMENTS

We would like to express our gratitude for the support received during this work, particularly at the Micro- and Nanoanalytics Facility (MNaF) Siegen. We would also like to acknowledge the assistance of Dr. Alexander Meledin at Thermo Fisher Scientific, who provided guidance on high-angle annular dark-field imaging.

REFERENCES

(1) Selvakumar, K.; Oh, T. H.; Wang, Y.; Sadhasivam, T.; Sadhasivam, S.; Swaminathan, M. Sonication Strategy for Anchoring Single Metal Atom Oxides (W, Cu, Co) on CeO_2-RGO for Boosting Electrocatalytic Oxygen Evolution Reaction. *Chemosphere* **2023**, *341*, No. 140012.

(2) Malali, P.; Muchharla, B.; Sadasivuni, K. K.; Cao, W.; Elsayed-Ali, H. E.; Adedeji, A.; Karoui, A.; Abdullah, A. M.; Spurgeon, J. M.; Kumar, B. Low Platinum-Loaded Molybdenum Co-Catalyst for the Hydrogen Evolution Reaction in Alkaline and Acidic Media. *Langmuir* **2022**, *38* (31), 9526−9531.

(3) Liu, L.; Corma, A. Metal Catalysts for Heterogeneous Catalysis: From Single Atoms to Nanoclusters and Nanoparticles. *Chem. Rev.* **2018**, *118* (10), 4981−5079.

(4) Li, J.; Yang, Z.; Li, Y.; Zhang, G. Advances in Single-Atom Catalysts: Design, Synthesis and Environmental Applications. *J. Hazard. Mater.* **2022**, *429*, No. 128285.

(5) Raja, A.; Son, N.; Swaminathan, M.; Kang, M. Synthesis of a Powerful Single Copper/Tungsten Atom Oxide Photocatalyst Dispersed on the Surface of a Reduced Graphene Oxide-Titanium Composite for H_2 Production and Pollutant Degradation. *Chem. Eng. J.* **2023**, *468*, No. 143740.

(6) Tyo, E. C.; Vajda, S. Catalysis by Clusters with Precise Numbers of Atoms. *Nat. Nanotechnol.* **2015**, *10* (7), 577−588.

(7) Hejazi, S.; Mehdi-pour, H.; Otieno, C. O.; Müller, J.; Pour-Ali, S.; Shahsanaei, M.; Sarabadani Tafreshi, S. S.; Butz, B.; Killian, M. S.; Mohajernia, S. Room-Temperature Defect-Engineered Titania: An Efficient Platform for Pt Single Atom Decoration for Photocatalytic H_2 Evolution. *Int. J. Hydrogen Energy* **2024**, *51*, 222−233.

(8) Wang, A.; Li, J.; Zhang, T. Heterogeneous Single-Atom Catalysis. *Nat. Rev. Chem.* **2018**, *2* (6), 65−81.
(9) Hejazi, S.; Pour-Ali, S.; Killian, M. S.; Mohajernia, S. One-Dimensional Suboxide TiO_2 Nanotubes for Electrodics Applications. *Electrochem. commun.* **2022**, *136*, No. 107246.
(10) Védrine, J. C. Importance, Features and Uses of Metal Oxide Catalysts in Heterogeneous Catalysis. *Chin. J. Catal.* **2019**, *40* (11), 1627−1636.
(11) Li, R.; Luo, L.; Ma, X.; Wu, W.; Wang, M.; Zeng, J. Single Atoms Supported on Metal Oxides for Energy Catalysis. *J. Mater. Chem. A* **2022**, *10* (11), 5717−5742.
(12) Lang, R.; Du, X.; Huang, Y.; Jiang, X.; Zhang, Q.; Guo, Y.; Liu, K.; Qiao, B.; Wang, A.; Zhang, T. Single-Atom Catalysts Based on the Metal−Oxide Interaction. *Chem. Rev.* **2020**, *120* (21), 11986−12043.
(13) Qiao, B.; Liang, J.-X.; Wang, A.; Xu, C.-Q.; Li, J.; Zhang, T.; Liu, J. J. Ultrastable Single-Atom Gold Catalysts with Strong Covalent Metal-Support Interaction (CMSI). *Nano Res.* **2015**, *8*, 2913−2924.
(14) Campbell, C. T. Electronic Perturbations. *Nat. Chem.* **2012**, *4* (8), 597−598.
(15) Bruix, A.; Rodriguez, J. A.; Ramírez, P. J.; Senanayake, S. D.; Evans, J.; Park, J. B.; Stacchiola, D.; Liu, P.; Hrbek, J.; Illas, F. A New Type of Strong Metal−Support Interaction and the Production of H_2 through the Transformation of Water on Pt/CeO_2 (111) and Pt/CeO x/TiO2 (110) Catalysts. *J. Am. Chem. Soc.* **2012**, *134* (21), 8968−8974.
(16) Raizada, P.; Soni, V.; Kumar, A.; Singh, P.; Parwaz Khan, A. A.; Asiri, A. M.; Thakur, V. K.; Nguyen, V.-H. Surface Defect Engineering of Metal Oxides Photocatalyst for Energy Application and Water Treatment. *J. Materiomics* **2021**, *7* (2), 388−418.
(17) Cao, H.; Wang, Q.; Zhang, Z.; Yan, H.-M.; Zhao, H.; Yang, H.; Liu, B.; Li, J.; Wang, Y.-G. Engineering Single-Atom Electrocatalysts for Enhancing Kinetics of Acidic Volmer Reaction. *J. Am. Chem. Soc.* **2023**, *145* (24), 13038−13047.
(18) Li, Z.; Ji, S.; Liu, Y.; Cao, X.; Tian, S.; Chen, Y.; Niu, Z.; Li, Y. Well-Defined Materials for Heterogeneous Catalysis: From Nanoparticles to Isolated Single-Atom Sites. *Chem. Rev.* **2020**, *120* (2), 623−682.
(19) Guo, J.; Liu, H.; Li, D.; Wang, J.; Djitcheu, X.; He, D.; Zhang, Q. A Minireview on the Synthesis of Single Atom Catalysts. *RSC Adv.* **2022**, *12* (15), 9373−9394.
(20) Di Liberto, G.; Maleki, F.; Pacchioni, G. PH Dependence of MgO, TiO_2, and γ-Al_2O_3 Surface Chemistry from First Principles. *J. Phys. Chem. C* **2022**, *126* (24), 10216−10223.
(21) Yadigarli, A.; Hartwich, P.; Onyenso, G.; Kowald, T.; Kübra Aktan, M.; Bream, A.; Killian, M. S. The Isoelectric Point of Metal Oxide Films Formed by Anodization. *Chemrxiv* **2023**.
(22) Liu, N.; Schneider, C.; Freitag, D.; Hartmann, M.; Venkatesan, U.; Müller, J.; Spiecker, E.; Schmuki, P. Black TiO2 Nanotubes: Cocatalyst-Free Open-Circuit Hydrogen Generation. *Nano Lett.* **2014**, *14* (6), 3309−3313.
(23) Bian, H.; Nguyen, N. T.; Yoo, J.; Hejazi, S.; Mohajernia, S.; Müller, J.; Spiecker, E.; Tsuchiya, H.; Tomanec, O.; Sanabria-Arenas, B. E.; et al. Forming a Highly Active, Homogeneously Alloyed AuPt Co-Catalyst Decoration on TiO_2 Nanotubes Directly during Anodic Growth. *ACS Appl. Mater. Interfaces* **2018**, *10* (21), 18220−18226.
(24) Mohajernia, S.; Andryskova, P.; Zoppellaro, G.; Hejazi, S.; Kment, S.; Zboril, R.; Schmidt, J.; Schmuki, P. Influence of Ti^{3+} Defect-Type on Heterogeneous Photocatalytic H_2 Evolution Activity of TiO_2. *J. Mater. Chem. A* **2020**, *8* (3), 1432−1442.
(25) Preočanin, T.; Kallay, N. Point of Zero Charge and Surface Charge Density of TiO_2 in Aqueous Electrolyte Solution as Obtained by Potentiometric Mass Titration. *Croat. Chem. Acta* **2006**, *79* (1), 95−106.
(26) Bertus, L. M.; Carcel, R. A. Prediction of TiO_2 and WO_3 Nanopowders Surface Charge by the Evaluation of Point of Zero Charge (PZC). *Env. Eng. Manag J.* **2011**, *10* (8), 1021−1026.
(27) Hejazi, S.; Mohajernia, S.; Osuagwu, B.; Zoppellaro, G.; Andryskova, P.; Tomanec, O.; Kment, S.; Zbořil, R.; Schmuki, P. On the Controlled Loading of Single Platinum Atoms as a Co-Catalyst on TiO_2 Anatase for Optimized Photocatalytic H_2 Generation. *Adv. Mater.* **2020**, *32* (16), No. 1908505.
(28) Obradović, M. D.; Stančić, Z. M.; Lačnjevac, U. Č.; Radmilović, V. V.; Gavrilović-Wohlmuther, A.; Radmilović, V. R.; Gojković, S. L. Electrochemical Oxidation of Ethanol on Palladium-Nickel Nanocatalyst in Alkaline Media. *Appl. Catal. B Environ.* **2016**, *189*, 110−118.
(29) Bancroft, G. M.; Adams, I.; Coatsworth, L. L.; Bennewitz, C. D.; Brown, J. D.; Westwood, W. D. ESCA Study of Sputtered Platinum Films. *Anal. Chem.* **1975**, *47* (3), 586−588.
(30) Zhang, L.; Zhu, J.; Li, X.; Mu, S.; Verpoort, F.; Xue, J.; Kou, Z.; Wang, J. Nurturing the Marriages of Single Atoms with Atomic Clusters and Nanoparticles for Better Heterogeneous Electrocatalysis. *Interdiscip. Mater.* **2022**, *1* (1), 51−87.
(31) Lang, R.; Xi, W.; Liu, J.-C.; Cui, Y.-T.; Li, T.; Lee, A. F.; Chen, F.; Chen, Y.; Li, L.; Li, L.; et al. Non Defect-Stabilized Thermally Stable Single-Atom Catalyst. *Nat. Commun.* **2019**, *10* (1), 234.
(32) Tran, N.-D.; Farnesi Camellone, M.; Fabris, S. Probing the Reactivity of Pt/Ceria Nanocatalysts toward Methanol Oxidation: From Ionic Single-Atom Sites to Metallic Nanoparticles. *J. Phys. Chem. C* **2018**, *122* (31), 17917−17927.
(33) Huang, D.; de Vera, G. A.; Chu, C.; Zhu, Q.; Stavitski, E.; Mao, J.; Xin, H.; Spies, J. A.; Schmuttenmaer, C. A.; Niu, J.; Haller, G. L.; Kim, J.-H. Single-Atom Pt Catalyst for Effective C−F Bond Activation via Hydrodefluorination. *ACS Catal.* **2018**, *8* (10), 9353−9358.
(34) Hejazi, S.; Nguyen, N. T.; Mazare, A.; Schmuki, P. Aminated TiO_2 Nanotubes as a Photoelectrochemical Water Splitting Photoanode. *Catal. Today* **2017**, *281*, 189−197.
(35) Altomare, M.; Nguyen, N. T.; Hejazi, S.; Schmuki, P. A Cocatalytic Electron-Transfer Cascade Site-Selectively Placed on TiO_2 Nanotubes Yields Enhanced Photocatalytic H_2 Evolution. *Adv. Funct. Mater.* **2018**, *28* (2), No. 1704259.
(36) Spieker, W. A.; Liu, J.; Hao, X.; Miller, J. T.; Kropf, A. J.; Regalbuto, J. R. An EXAFS Study of the Coordination Chemistry of Hydrogen Hexachloroplatinate (IV): 2. Speciation of Complexes Adsorbed onto Alumina. *Appl. Catal. A Gen.* **2003**, *243* (1), 53−66.
(37) Shelimov, B.; Lambert, J.-F.; Che, M.; Didillon, B. Application of NMR to Interfacial Coordination Chemistry: A ^{195}Pt NMR Study of the Interaction of Hexachloroplatinic Acid Aqueous Solutions with Alumina. *J. Am. Chem. Soc.* **1999**, *121* (3), 545−556.
(38) Kriek, R. J.; Mogwase, B. M. S.; Vorster, S. W. Relation of the Electrochemical Interplay between H_2PtCl_6 and $H_2O/H_3O^+/H_2^+$ and the Hydrogen-evolution Reaction. *Electrochem. Sci. Adv.* **2022**, *2* (2), No. e2100041.

https://doi.org/10.1021/acs.langmuir.3c03316
Langmuir 2024, 40, 4661−4668